

Dudin et al., <http://www.jcb.org/cgi/content/full/jcb.201411124/DC1>

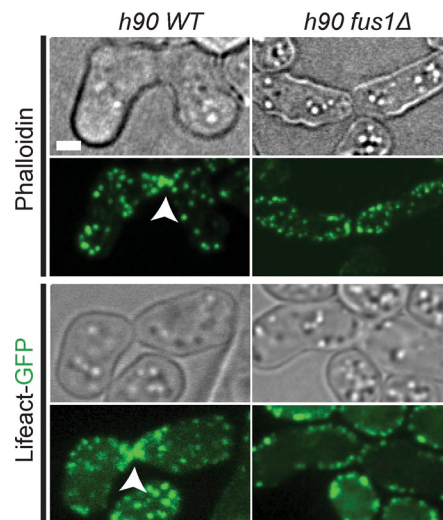


Figure S1. Fus1-dependent actin accumulation at the prospective fusion site. (Related to Fig. 1.) Images of homothallic wild-type (WT) *h90* strains (left) fixed and stained with Alex Fluor–phalloidin (top) or live expressing LifeAct-GFP. The arrowheads indicate actin accumulation at the fusion site. (right) In contrast, no actin accumulation is observed in *h90 fus1Δ* strains. Bar, 1 μ m.

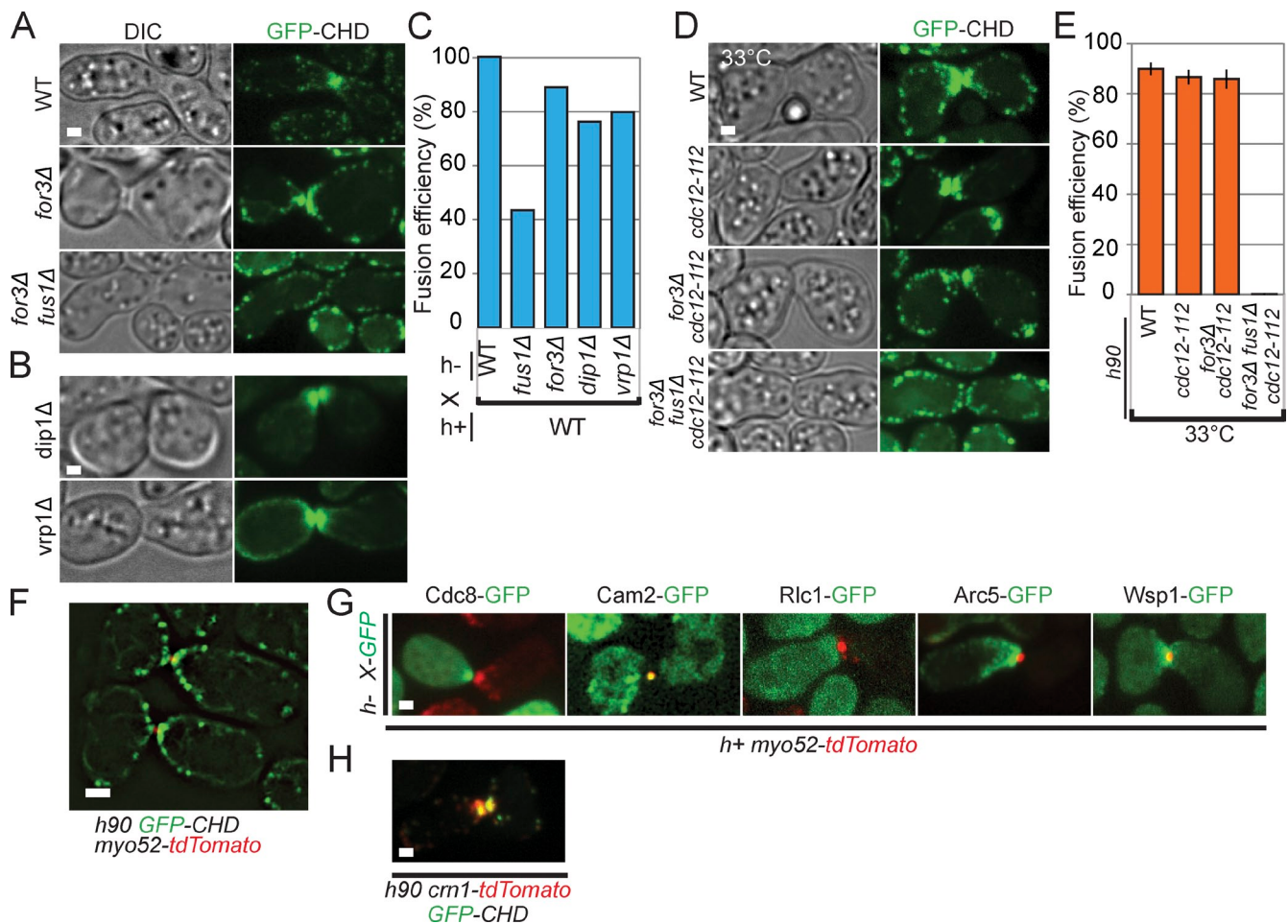


Figure S2. Fusion focus formation is independent of formins For3 and Cdc12 and of actin patch components. (Related to Fig. 2.) (A) Homothallic *h90* wild-type (WT), *for3* Δ , and *for3* Δ *fus1* Δ strains expressing GFP-CHD. An actin focus forms in *for3* Δ but not in *for3* Δ *fus1* Δ . (B) Homothallic *h90* *dip1* Δ and *vrp1* Δ strains expressing GFP-CHD, in which the fusion focus forms normally. (C) Fusion efficiency of indicated heterothallic crosses, $n > 90$. (D) Homothallic *h90* wild-type, *cdc12-112*, *cdc12-112 for3* Δ , and *cdc12-112 for3* Δ *fus1* Δ strains expressing GFP-CHD imaged at 33°C. An actin focus forms in all cases, except upon *fus1* deletion. Note the presence of some aberrant actin structures in the *cdc12-112 for3* Δ double mutant. (E) Fusion efficiency of homothallic *h90* wild-type, *cdc12-112*, *cdc12-112 for3* Δ , and *cdc12-112 for3* Δ *fus1* Δ mutants at 33°C. For3 and Cdc12 do not contribute during cell-cell fusion. Error bars are standard deviations. (F) 3D SIM of GFP-CHD and Myo52-tdTomato colocalization in homothallic *h90* wild type. This image represents the same cell pair as shown in Fig. 2 F, after which time-lapse imaging of only the GFP channel was acquired. (G) Heterothallic *h-* strains expressing indicated GFP fusions crossed to *h+* *myo52-tdTomato* cells. Cdc8 tropomyosin and Cam2 calmodulin form a dot at the fusion site, but not Rlc1, Arc5, or Wsp1. (H) Homothallic *h90 crn1-tdTomato* GFP-CHD. Crn1 coronin decorates the fusion focus. DIC, differential interference contrast. Bars, 1 μ m.

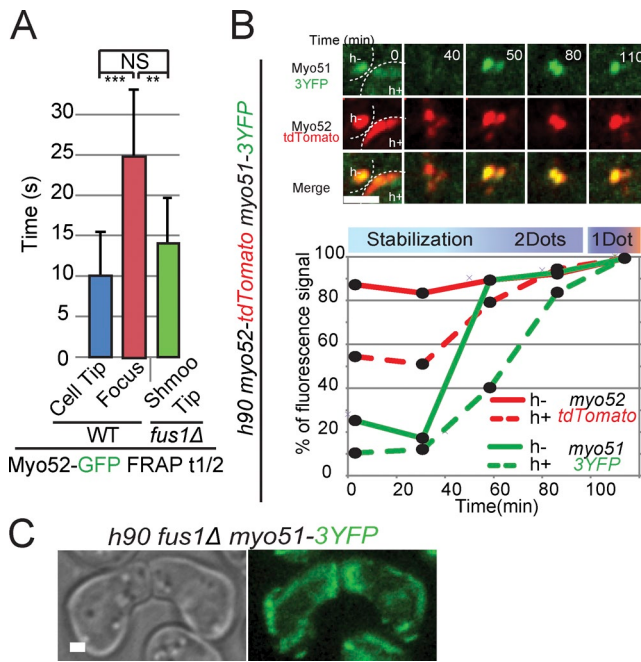


Figure S3. Type V myosin localization and dynamics define multiple steps in the formation of the fusion focus. (Related to Fig. 4.) (A) Mean FRAP recovery half-times of Myo52-GFP at the cell tip of vegetative growing cells or during cell–cell fusion in presence or absence of Fus1. Myo52 lower mobility at the fusion focus depends on Fus1. Note that the half-time values measured with Myo52-GFP are somewhat larger than those measured using Myo52-tdTomato (see Fig. 3 C), but the differences between focus and cell tip are similar. *t* test, ***, P = 6.9×10^{-10} ; **, P = 1.3×10^{-4} ; n > 12 for each category. Error bars are standard deviations. WT, wild type. (B, top) Detail of the contact zone of a homothallic h90 *myo52-tdTomato myo51-3YFP* mating pair. (bottom) The graph shows Myo52 and Myo51 fluorescence intensities normalized to the maximum of each fluorophore. Myo51 and Myo52 focalize first in the h⁻ cell. This is one representative example out of five such measured mating pairs. Cell contours are shown with dotted lines. (C) Homothallic h90 *fus1 Δ myo51-3YFP* strain. Myo51 accumulates as a crescent at the shmoo tip in absence of Fus1. Bars, 1 μ m.

Table S1. Strains used in this study

| Strain number | Genotype | Source |
|---------------|---|------------------------|
| Fig. 1 | | |
| 2514 | <i>h90 p^{map3}-tdTomato-ura4+ nmt41::GFP-CHD-leu⁺ ade6⁻ leu1-32 ura4-D18</i> | This study |
| 2515 | <i>h90 myo52-tdTomato-natMX nmt41::GFP-CHD-leu⁺ ade6⁻ leu1-32 ura4-D18</i> | This study |
| 2516 | <i>h90 fus1::LEU2 p^{map3}-tdTomato-ura4⁺ nmt41::GFP-CHD-leu⁺ ade6⁻ leu1-32 ura4-D18</i> | This study |
| Fig. 2 | | |
| 2515 | <i>h90 myo52-tdTomato-natMX nmt41::GFP-CHD-leu⁺ ade6⁻ leu1-32 ura4-D18</i> | This study |
| 2517 | <i>h90 fus1-sfGFP-kanMX p^{map3}-tdTomato-ura4⁺ ade6⁺ leu1⁺ ura4-D18</i> | This study |
| 2518 | <i>h⁺ fus1-sfGFP-kanMX myo52-tdTomato-natMX</i> | This study |
| 2519 | <i>h⁻ fus1-sfGFP-kanMX myo52-tdTomato-natMX</i> | This study |
| 2520 | <i>h90 myo52-GFP-kanMX leu1-32</i> | This study |
| 2521 | <i>h90 fus1::LEU2 myo52-GFP-kanMX leu1-32</i> | This study |
| 740 | <i>h⁺ myo52-tdTomato-natMX ade6-M216 leu1-32 ura4-D18</i> | Laboratory stock |
| 2522 | <i>h90 for3::kanMX nmt41::GFP-CHD-leu⁺ ade6⁻ leu1-32 ura4-D18</i> | This study |
| 2516 | <i>h90 fus1::LEU2 p^{map3}-tdTomato-ura4⁺ nmt41::GFP-CHD-leu⁺ ade6⁻ leu1-32 ura4-D18</i> | This study |
| 2587 | <i>h90 for3::kanMX fus1::LEU2 nmt41::GFP-CHD-leu⁺ ade6⁻ leu1-32 ura4-D18</i> | This study |
| 2523 | <i>h⁻ cdc12-3GFP-kanMX myo52-tomato-natMX ade6⁻ leu1-32 ura4-D18</i> | This study |
| 2524 | <i>h⁺ cdc12-3GFP-kanMX myo52-tomato-natMX ade6⁻ leu1-32 ura4-D18</i> | This study |
| 2525 | <i>h⁻ P^{cdc15}-mEGFP-cdc15:: kanMX myo52-tdTomato-natMX ade6⁻ leu1-32 ura4-D18</i> | This study |
| 2526 | <i>h⁺ P^{cdc15}-5-mEGFP-cdc15:: kanMX myo52-tdTomato-natMX ade6⁻ leu1-32 ura4-D18</i> | This study |
| 2527 | <i>h⁻ for3-3GFP-kanMX myo52-tdTomato-natMX ade6⁻ leu1-32 ura4-D18</i> | This study |
| 2528 | <i>h⁺ for3-3GFP-kanMX myo52-tdTomato-natMX ade6⁻ leu1-32 ura4-D18</i> | This study |
| 2529 | <i>h90 myo52-tdTomato-natMX myo51-3YFP-kanMX leu1-32 ura4-D18</i> | This study |
| 2530 | <i>h⁻ kanMX-P^{myo1}-mGFP-my01 myo52-tdTomato-natMX ade6⁻ leu1-32 ura4-D18</i> | This study |
| 2531 | <i>h⁺ kanMX-P^{myo1}-mGFP-my01 myo52-tdTomato-natMX ade6⁻ leu1-32 ura4-D18</i> | This study |
| 2532 | <i>h⁻ myo52-tdTomato-natMX dip1-GFP-kanMX ade6-M216 leu1-32 ura4-D18</i> | This study |
| 2533 | <i>h⁺ myo52-tdTomato-natMX dip1-GFP-kanMX ade6-M216 leu1-32 ura4-D18</i> | This study |
| Fig. 3 | | |
| 2515 | <i>h90 myo52-tdTomato-NatMX nmt41::GFP-CHD-leu⁺ ade6⁻ leu1-32 ura4-D18</i> | This study |
| 2534 | <i>h⁻ myo52-GFP-kanMX leu1-32</i> | This study |
| 2535 | <i>h90 myo52-tdTomato-natMX p^{map3}-GFP-ura4⁺ ade6-M216 leu1-32 ura4-D18</i> | This study |
| 952 | <i>h⁻ myo52-tdTomato-natMX ade6-M216 leu1-32 ura4-D18</i> | Laboratory stock |
| 740 | <i>h⁺ myo52-tdTomato-natMX ade6-M216 leu1-32 ura4-D18</i> | Laboratory stock |
| 1273 | <i>h⁻ nmt41::GFP-CHD-leu⁺ ade6-M216 leu1-32 ura4-D18</i> | Laboratory stock |
| 2594 | <i>h⁺ nmt41::GFP-CHD-leu⁺ ade6-M216 leu1-32 ura4-D18</i> | This study |
| 2529 | <i>h90 myo52-tdTomato-natMX myo51-3YFP-kanMX leu1-32 ura4-D18</i> | This study |
| 2518 | <i>h⁺ fus1-sfGFP-kanMX myo52-tdTomato-natMX</i> | This study |
| 2519 | <i>h⁻ fus1-sfGFP-kanMX myo52-tdTomato-natMX</i> | This study |
| Fig. 4 | | |
| 1372 | <i>h⁻ WT (972)</i> | Laboratory stock |
| 1371 | <i>h⁺ WT (975)</i> | Laboratory stock |
| 2536 | <i>h⁻ myo52::ura4⁺ leu1⁻ ura4-</i> | This study |
| 1923 | <i>h⁺ myo52::ura4⁺ leu1⁻ ura4-</i> | Laboratory stock |
| 1532 | <i>h⁻ myo51::ura4⁺ ade6-M216 leu1-32 ura4-D18</i> | Laboratory stock |
| 2537 | <i>h⁺ myo51::ura4⁺ leu1-32 ura4-D18</i> | This study |
| 2538 | <i>h⁻ myo52::ura4⁺ myo51::ura4⁺ ade6⁻ ura4-</i> | This study |
| 2539 | <i>h⁺ myo52::ura4⁺ myo51::ura4⁺ leu1⁻ ura4-</i> | This study |
| 1024 | <i>h⁻ fus1::LEU2 ade6-</i> | Laboratory stock |
| 1025 | <i>h⁺ fus1::LEU2 ade6-</i> | Laboratory stock |
| 1273 | <i>h⁻ nmt41::GFP-CHD-leu⁺ ade6-M216 leu1-32 ura4-D18</i> | Laboratory stock |
| 663 | <i>h⁺ myo51::ura4⁺ myo52::ura4⁺ nmt41::GFP-CHD-leu⁺ ade6-M216 leu1-32 ura4-D18</i> | Laboratory stock |
| 2517 | <i>h90 fus1-sfGFP-kanMX p^{map3}-tdTomato-ura4⁺ ade6⁺ leu1⁺ ura4-D18</i> | This study |
| 2541 | <i>h90 myo52::ura4⁺ fus1-sfGFP leu1⁻ ura4-</i> | This study |
| 2542 | <i>h90 myo51::ura4⁺ fus1-sfGFP leu1⁻ ura4-</i> | This study |
| 2543 | <i>h90 myo52::ura4⁺ myo51::ura4⁺ fus1-sfGFP leu1⁻ ura4-</i> | This study |
| 2544 | <i>h90 myo52::ura4⁺ leu1⁻ ura4-</i> | This study |
| 2545 | <i>h90 myo51::ura4⁺ leu1⁻ ura4-</i> | This study |
| 1396 | <i>h90 WT (968)</i> | Laboratory stock |
| 2546 | <i>h⁻ myo52^{tail}-tdTomato-kanMX ade6-M210 leu1-32 ura4-D18</i> | Lo Presti et al., 2012 |

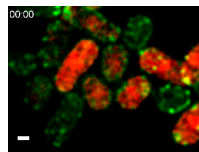
Table S1. Strains used in this study (Continued)

| Strain number | Genotype | Source |
|----------------|--|-----------------------------|
| 2005 | h^- <i>myo51^{Δtail}-3GFP-ura4⁺ ade6-M216 leu1⁻ ura4</i> | Lo Presti et al., 2012 |
| Fig. 5 | | |
| 2547 | h^- <i>agn1-GFP-kanMX myo52-tdTomato-natMX ade6-M216 leu1-32 ura4-D18</i> | This study |
| 2548 | h^+ <i>agn1-GFP-kanMX myo52-tdTomato-natMX ade6-M216 leu1-32 ura4-D18</i> | This study |
| 2549 | h^- <i>agn2-GFP-kanMX myo52-tdTomato-natMX ade6-M216 leu1-32 ura4-D18</i> | This study |
| 2550 | h^+ <i>agn2-GFP-kanMX myo52-tdTomato-natMX ade6-M216 leu1-32 ura4-D18</i> | This study |
| 2551 | h^- <i>eng1-GFP-kanMX myo52-tdTomato-natMX ade6-M216 leu1-32 ura4-D18</i> | This study |
| 2552 | h^+ <i>eng1-GFP-kanMX myo52-tdTomato-natMX ade6-M216 leu1-32 ura4-D18</i> | This study |
| 2553 | h^- <i>eng2-GFP-kanMX myo52-tdTomato-natMX ade6-M216 leu1-32 ura4-D18</i> | This study |
| 2554 | h^+ <i>eng2-GFP-kanMX myo52-tdTomato-natMX ade6-M216 leu1-32 ura4-D18</i> | This study |
| 2555 | h^- <i>exg1-GFP::kanMX myo52-tdTomato-natMX ade6-M216 leu1-32 ura4-D18</i> | This study |
| 2556 | h^+ <i>exg1-GFP::kanMX myo52-tdTomato-natMX ade6-M216 leu1-32 ura4-D18</i> | This study |
| 2557 | h^- <i>exg2-GFP::kanMX myo52-tdTomato-natMX ade6-M216 leu1-32 ura4-D18</i> | This study |
| 2558 | h^+ <i>exg2-GFP::kanMX myo52-tdTomato-natMX ade6-M216 leu1-32 ura4-D18</i> | This study |
| 2559 | h^- <i>exg3-GFP::kanMX myo52-tdTomato-natMX ade6-M216 leu1-32 ura4-D18</i> | This study |
| 2560 | h^+ <i>exg3-GFP::kanMX myo52-tdTomato-natMX ade6-M216 leu1-32 ura4-D18</i> | This study |
| 2561 | h^- <i>agn1::ura4⁺ myo52-tdTomato-natMX ade6-M216 leu1-32 ura4-D18</i> | This study |
| 2562 | h^- <i>agn2::kanMX myo52-tdTomato-natMX ade6-M216 leu1-32 ura4-D18</i> | This study |
| 2563 | h^- <i>eng1::kanMX myo52-tdTomato-natMX ade6-M216 leu1-32 ura4-D18</i> | This study |
| 2564 | h^- <i>eng2::kanMX myo52-tdTomato-natMX ade6-M216 leu1-32 ura4-D18</i> | This study |
| 2195 | h^- <i>exg1::kanMX leu1-32</i> | Dueñas-Santero et al., 2010 |
| 2565 | h^- <i>exg2::kanMX myo52-tdTomato-natMX ade6-M216 leu1-32 ura4-D18</i> | This study |
| 2566 | h^- <i>exg3::kanMX myo52-tdTomato-natMX ade6-M216 leu1-32 ura4-D18</i> | This study |
| 2567 | h^- <i>eng2::kanMX agn2::kanMX myo52-tdTomato-natMX ade6-M216 leu1-32 ura4-D18</i> | This study |
| 2595 | h^+ <i>exg3::kanMX agn2::kanMX myo52-tdTomato-natMX ade6-M216 leu1-32 ura4-D18</i> | This study |
| 2568 | h^- <i>exg3::kanMX agn2::kanMX myo52-tdTomato-natMX ade6-M216 leu1-32 ura4-D18</i> | This study |
| 2569 | h^- <i>exg3::kanMX eng2::kanMX myo52-tdTomato-natMX ade6-M216 leu1-32 ura4-D18</i> | This study |
| 2570 | h^- <i>exg3::kanMX eng2::kanMX agn2::kanMX ade6-M216 leu1-32 ura4-D18</i> | This study |
| 1088 | h^- <i>bgs1::ura4⁺ p^{bgs1}::GFP-bgs1-leu1⁺ leu1-32 ura4-D18 his3-D1</i> | Cortés et al., 2002 |
| 806 | h^- <i>bgs4::ura4⁺ p^{bgs4}::GFP-bgs4-leu1⁺ leu1⁻ ura4-D18</i> | Cortés et al., 2005 |
| 2571 | $h90$ <i>agn2-sfGFP-kanMX myo52-tdTomato-natMX ade6-M216 leu1-32 ura4-D18</i> | This study |
| 2572 | $h90$ <i>eng2-sfGFP-kanMX myo52-tdTomato-natMX ade6-M216 leu1-32 ura4-D18</i> | This study |
| 2573 | $h90$ <i>exg3-sfGFP-kanMX myo52-tdTomato-natMX ade6-M216 leu1-32 ura4-D18</i> | This study |
| 2574 | $h90$ <i>agn2-sfGFP-kanMX myo52-tdTomato-natMX fus1Δ::LEU2 ade6⁺ leu1-32 ura4-294</i> | This study |
| 2575 | $h90$ <i>eng2-sfGFP-kanMX myo52-tdTomato-natMX fus1Δ::LEU2 ade6⁺ leu1-32 ura4-294</i> | This study |
| 2576 | $h90$ <i>exg3-sfGFP-kanMX myo52-tdTomato-natMX fus1Δ::LEU2 ade6⁺ leu1-32 ura4-294</i> | This study |
| 2577 | $h90$ <i>myo52::ura4⁺ myo51::ura4⁺ agn2-sfGFP-kanMX leu1⁻ ura4-</i> | This study |
| 2578 | $h90$ <i>myo52::ura4⁺ myo51::ura4⁺ eng2-sfGFP-kanMX leu1⁻ ura4-</i> | This study |
| 2579 | $h90$ <i>myo52::ura4⁺ myo51::ura4⁺ exg3-sfGFP-kanMX leu1⁻ ura4-</i> | This study |
| 952 | h^- <i>myo52-tdTomato-natMX ade6-M216 leu1-32 ura4-D18</i> | Laboratory stock |
| 2580 | h^+ <i>myo51^{Δtail}-12myc-ura4⁺ agn2-sfGFP-kanMX ade6⁺ leu1-32 ura4-D18</i> | This study |
| 2581 | h^+ <i>myo52^{Δtail}-tdTomato-kanMX agn2-sfGFP-kanMX ade6-M216 leu1-32 ura4-D18</i> | This study |
| 2582 | h^+ <i>myo51^{Δtail}-12myc-ura4⁺ eng2-sfGFP-kanMX ade6⁺ leu1-32 ura4-D18</i> | This study |
| 2583 | h^+ <i>myo52^{Δtail}-tdTomato-kanMX eng2-sfGFP-kanMX ade6-M216 leu1-32 ura4-D18</i> | This study |
| 2584 | h^+ <i>myo51^{Δtail}-12myc-ura4⁺ exg3-sfGFP-kanMX ade6⁺ leu1-32 ura4-294</i> | This study |
| 2585 | h^+ <i>myo52^{Δtail}-tdTomato-kanMX exg3-sfGFP-kanMX ade6-M216 leu1-32 ura4-D18</i> | This study |
| Fig. S1 | | |
| 1396 | $h90$ WT [968] | Laboratory stock |
| 1442 | $h90$ <i>fus1::LEU2 leu1⁻ ura4-D18</i> | Laboratory stock |
| 2596 | $h90$ <i>nmt41::lifeact-GFP-leu⁺ ade6⁻ leu1-32 ura4-D18</i> | This study |
| 2586 | $h90$ <i>fus1::LEU2 nmt41::lifeact-GFP ade6⁻ leu1-32 ura4-D18</i> | This study |
| Fig. S2 | | |
| 2514 | $h90$ <i>p^{map3}-tdTomato-ura4⁺ nmt41::GFP-CHD-leu⁺ ade6⁻ leu1-32 ura4-D18</i> | This study |
| 2522 | $h90$ <i>for3::kanMX nmt41::GFP-CHD-leu⁺ ade6⁻ leu1-32 ura4-D18</i> | This study |
| 2587 | $h90$ <i>for3::kanMX fus1::LEU2 nmt41::GFP-CHD-leu⁺ ade6⁻ leu1-32 ura4-D18</i> | This study |
| 2597 | $h90$ <i>dip1::natMX nmt41::GFP-CHD leu⁺ ade6⁻ leu1-32 ura4-D18</i> | This study |
| 2598 | $h90$ <i>vrp1::kanMX nmt41::GFP-CHD ade6-M216 leu1-32 ura4-D18 his3-D1</i> | This study |
| 2599 | h^- <i>vrp1::kanMX myo52-tdTomato-natMX ade6⁻ leu1-32 ura4-D18</i> | This study |
| 1944 | h^- <i>dip1::natMX ade6-M216 leu1-32 ura4-D18</i> | Basu and Chang, 2011 |

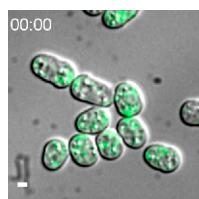
Table S1. Strains used in this study (Continued)

| Strain number | Genotype | Source |
|----------------|--|---------------------------|
| 1055 | <i>h⁻ for3::kanMX ade6⁻ leu1-32 ura4-D18</i> | Laboratory stock |
| 2588 | <i>h90 cdc12-112 nmt41::GFP-CHD-leu<sup+< sup=""> ade6⁻ leu1-32 ura4-D18</sup+<></i> | This study |
| 2589 | <i>h90 for3::kanMX cdc12-112 nmt41::GFP-CHD-leu<sup+< sup=""> ade6⁻ leu1⁻ ura4-D18</sup+<></i> | This study |
| 2590 | <i>h90 for3::kanMX cdc12-112 fus1::LEU2 nmt41::GFP-CHD-leu<sup+< sup=""> ade6⁻ leu1-32 ura4-D18</sup+<></i> | This study |
| 2173 | <i>h⁻ leu1::nmt41-GFP-cdc8-ura4⁺ ura4-D18</i> | Skau et al., 2011 |
| 2591 | <i>h⁻ rlc1-GFP-kanMX leu1⁻ ura4-</i> | This study |
| 2163 | <i>h⁻ arc5-mGFP-kanMX ade6-M216 leu1-32 ura4-D18 his3-D1</i> | Arasada and Pollard, 2011 |
| 2194 | <i>h90 cam2::ura4⁺ ade6<<cam2-GFP leu1-32 ura4-D18</i> | Itadani et al., 2006 |
| 2161 | <i>h⁻ kanMX-P^{wsp1}-mGFP-wsp1 ade6-M216 leu1-32 ura4-D18 his3-D1</i> | Arasada and Pollard, 2011 |
| 2592 | <i>h90 crn1-tdTomato-natMX nmt41::GFP-CHD-leu⁺ ade6⁻ leu1-32 ura4-D18</i> | This study |
| 740 | <i>h⁺ myo52-tdTomato-natMX ade6-M216 leu1-32 ura4-D18</i> | Laboratory stock |
| Fig. S3 | | |
| 2520 | <i>h90 myo52-GFP-kanMX leu1-32</i> | This study |
| 2521 | <i>h90 fus1::LEU2 myo52-GFP-kanMX leu1-32</i> | This study |
| 2529 | <i>h90 myo52-tdTomato-natMX myo51-3YFP-kanMX leu1-32 ura4-D18</i> | This study |
| 2593 | <i>h90 myo51-3YFP-kanMX fus1::LEU1 ade6-M216 leu1-32 ura4-D18</i> | This study |

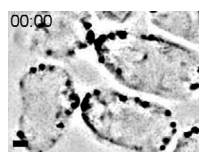
All tagging constructs are in frame after the last codon of the gene or before the first one and integrated at the endogenous genomic locus. All deletions are replacements of the complete gene ORF with the selectable marker. The *p^{map3}*-driven transgenes are integrated in the *map3* promoter locus. WT, wild type.



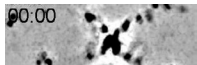
Video 1. An actin fusion focus forms before cell fusion. (Related to Fig. 1.) Time lapse of homothallic *h90 p^{map3}:tdTomato GFP-CHD* strain obtained by wide field microscopy and deconvolved using the DeltaVision platform (Olympus IX-71; Applied Precision). CHD-GFP is shown in green; tdTomato in red. Time interval is 2 min. The video is sped up sevenfold. Three distinct mating pairs can be seen fusing during the course of the video. Note formation of the fusion focus before fusion, entry of the red signal in the *h⁺* cell at fusion time and focus disassembly after fusion. Bar, 1 μm.



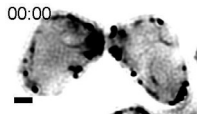
Video 2. Absence of actin fusion focus in *fus1Δ*. (Related to Fig. 1.) Time-lapse of homothallic *h90 fus1Δ GFP-CHD* strain obtained by wide field microscopy and deconvolved using the DeltaVision platform (Olympus IX-71; Applied Precision). CHD-GFP is shown in green; differential interference contrast image in gray. Time interval is 2 min. The video is sped up sevenfold. Four distinct mating pairs can be seen, all of which fail to fuse. Instead, mating partners keep growing in a polarized fashion toward each other. Actin structures, likely actin patches can be seen dynamically localizing at the shmoos tip, but no long-lasting actin focus is observed. Note the GFP-CHD channel has been contrasted to allow visibility on the differential interference contrast image. Bar, 1 μm.



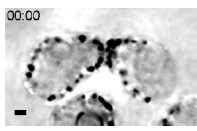
Video 3. The actin fusion focus visualized by 3D SIM. (Related to Fig. 2.) Time-lapse of GFP-CHD in homothallic *h90 WT GFP-CHD myo52-tdTomato* cells. Only the GFP-CHD channel is shown. Inverted images are shown obtained using the SIM setup (Eclipse T1; Nikon). Time interval is 6 s. The video is sped up sevenfold. Long linear dynamic actin cables are observed originating from the zone of cell-cell contact. Contrast was adjusted to optimize cable visualization. Bar, 1 μm.



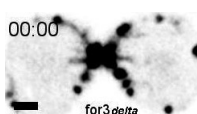
Video 4. The actin fusion focus visualized by 3D SIM in *for3Δ*. (Related to Fig. 2.) Time-lapse of homothallic *h90 for3Δ* GFP-CHD cells. Inverted images are shown obtained using the SIM setup (Eclipse T1; Nikon). Time interval is 3 s. The video is sped up sevenfold. Short linear dynamic actin cables are observed originating from the zone of cell-cell contact. Contrast was adjusted to optimize cable visualization. Bar, 1 μ m.



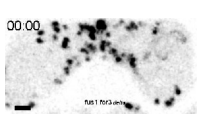
Video 5. Actin at the zone of cell-cell contact visualized by 3D SIM in *fus1Δ*. (Related to Fig. 2.) Time-lapse of homothallic *h90 fus1Δ* GFP-CHD cells. Inverted images are shown obtained using the SIM setup (Eclipse T1; Nikon). Time interval is 3 s. The video is sped up sevenfold. Long dynamic actin cables are observed emanating from a broad region at the cell-cell contact site. Contrast was adjusted to optimize cable visualization. Bar, 1 μ m.



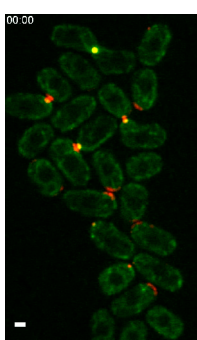
Video 6. Actin at the zone of cell-cell contact visualized by 3D SIM in *fus1Δ for3Δ*. (Related to Fig. 2.) Time-lapse of homothallic *h90 fus1Δ for3Δ* GFP-CHD cells obtained using the SIM setup (Eclipse T1; Nikon). Inverted images are shown. Time interval is 3 s. The video is sped up sevenfold. No actin cables were observed; however, a perinuclear actin ring is seen. Note that only part of this ring is visible because only a single focal plane is shown. Bar, 1 μ m.



Video 7. The actin fusion focus visualized by scanning confocal microscopy in WT and *for3Δ*. (Related to Fig. 2.) Images of homothallic *h90* WT GFP-CHD *myo52-tdTomato* (left) and *h90 for3Δ* GFP-CHD (right) cells obtained by laser-scanning confocal microscopy (LSM 710; Carl Zeiss). Only the GFP-CHD signal was imaged to minimize the time interval (2 s). The video is sped up sevenfold. Long and short actin cables are observed originating from the zone of cell-cell contact in WT cells, and short linear actin cables are observed in *for3Δ* cells. Contrast was adjusted to optimize cable visualization. Bar, 1 μ m.



Video 8. Actin at the zone of cell-cell contact visualized by scanning confocal microscopy in *fus1Δ* and *fus1Δ for3Δ*. (Related to Fig. 2.) Images of homothallic *h90 fus1Δ* GFP-CHD (left) and *h90 fus1Δ for3Δ* GFP-CHD (right) cells obtained by laser-scanning confocal microscopy (LSM 710; Carl Zeiss). Time interval is 2 s. The video is sped up sevenfold. Long dynamic, unfocused actin cables are observed in *fus1Δ*. No actin cables were observed in *fus1Δ for3Δ*. Contrast was adjusted to optimize cable visualization. Bar, 1 μ m.



Video 9. Asymmetric maturation of the fusion focus. (Related to Fig. 3.) Time-lapse of homothallic *h90* WT *myo52-tdTomato* *myo51-3YFP* obtained by spinning disk microscopy (UltraVIEW system [PerkinElmer] on DMI4000B [Leica]). *Myo52-tdTomato* is shown in red; *Myo51-3YFP* is shown in green. Time interval is 1.3 s. The video is sped up sevenfold. The video shows five mating pairs at distinct stages of the fusion process. Pair 1 shows *Myo52-tdTomato* crescent in both partner cells, with the bottom cell structure focalizing in the course of the video. Pairs 2, 3, and 4 show asymmetric structures, with *Myo51-3YFP* strongly localized with *Myo52-tdTomato* in only one of the two mating partners. Note how the *Myo52-tdTomato* structure in the other cell moves at the contact zone relative to that stable focus. In the course of the video, *Myo51-3YFP* accumulates in the focus of the bottom cell of pair 4. Finally, pair 5 shows a single *Myo51-Myo52* focus at the fusion site, which disassembles in the course of the video. Bar, 1 μ m.

References

- Arasada, R., and T.D. Pollard. 2011. Distinct roles for F-BAR proteins Cdc15p and Bzz1p in actin polymerization at sites of endocytosis in fission yeast. *Curr. Biol.* 21:1450–1459. <http://dx.doi.org/10.1016/j.cub.2011.07.046>
- Basu, R., and F. Chang. 2011. Characterization of dip1p reveals a switch in Arp2/3-dependent actin assembly for fission yeast endocytosis. *Curr. Biol.* 21:905–916. <http://dx.doi.org/10.1016/j.cub.2011.04.047>
- Cortés, J.C., J. Ishiguro, A. Durán, and J.C. Ribas. 2002. Localization of the (1,3)beta-D-glucan synthase catalytic subunit homologue Bgs1p/Cps1p from fission yeast suggests that it is involved in septation, polarized growth, mating, spore wall formation and spore germination. *J. Cell Sci.* 115:4081–4096. <http://dx.doi.org/10.1242/jcs.00085>
- Cortés, J.C., E. Carnero, J. Ishiguro, Y. Sánchez, A. Durán, and J.C. Ribas. 2005. The novel fission yeast (1,3)beta-D-glucan synthase catalytic subunit Bgs4p is essential during both cytokinesis and polarized growth. *J. Cell Sci.* 118:157–174. <http://dx.doi.org/10.1242/jcs.01585>
- Dueñas-Santero, E., A.B. Martín-Cuadrado, T. Fontaine, J.P. Latgé, F. del Rey, and C. Vázquez de Aldana. 2010. Characterization of glycoside hydrolase family 5 proteins in *Schizosaccharomyces pombe*. *Eukaryot. Cell.* 9:1650–1660. <http://dx.doi.org/10.1128/EC.00187-10>
- Itadani, A., T. Nakamura, and C. Shimoda. 2006. Localization of type I myosin and F-actin to the leading edge region of the forespore membrane in *Schizosaccharomyces pombe*. *Cell Struct. Funct.* 31:181–195. <http://dx.doi.org/10.1247/csf.06027>
- Lo Presti, L., F. Chang, and S.G. Martin. 2012. Myosin Vs organize actin cables in fission yeast. *Mol. Biol. Cell.* 23:4579–4591. <http://dx.doi.org/10.1091/mbc.E12-07-0499>
- Skau, C.T., D.S. Courson, A.J. Bestul, J.D. Winkelman, R.S. Rock, V. Sirotkin, and D.R. Kovar. 2011. Actin filament bundling by fimbrin is important for endocytosis, cytokinesis, and polarization in fission yeast. *J. Biol. Chem.* 286:26964–26977. <http://dx.doi.org/10.1074/jbc.M111.239004>